Int. J. Electrochem. Sci., 16 **(2021)** Article Number: 211021, doi: 10.20964/2021.10.28

International Journal of
ELECTROCHEMICAL
SCIENCE
www.electrochemsci.org

Short Communication

Preparation of electrochemical sensor assisted unmanned aerial vehicles system for SO_2, O_3, NO_2, CO and PM2.5/PM10 detection in air

Rongqiang Guan, Jing Yu[*], *Mingyue Li, Jingjing Yan, Zichao Liu*

Jilin Engineering Normal University, Changchun, Jinlin, 130052, P.R. China
[*]E-mail: jingyu_0c14@163.com

Received: 30 May 2021 / *Accepted:* 22 July 2021 / *Published:* 10 September 2021

The spatial and especially vertical monitoring of atmospheric pollutants is of great significance to the analysis and prevention of air pollution. It is also a useful supplement to the current monitoring method which is mainly based on ground monitoring stations. Small UAVs offer a new way of vertical monitoring of air pollution. In this study, an electrochemical sensor incorporated unmanned aerial vehicles (UAV) platform was proposed, which can detect pollution at vertical heights, and has been used for PM2.5, PM10 and 4 pollutants (SO_2, O_3, NO_2, CO) at different heights. Based on this monitoring data, the vertical distribution characteristics as well as the statistical correlation of PM2.5 and its pollutants were analyzed. The experimental results show that PM2.5 concentration increases with height in the larger integrated industrial areas, while it decreases and then increases near the small-scale industrial and residential areas. The trends of PM10 and PM2.5 are basically consistent. In the vertical direction, the maximum values of CO and SO_2 always appear near the ground and then start to decrease, and NO_2 increases with the height.

Keywords: UVA system; Electrochemical gas sensor; Pollutants; Atmospheric pollution; Spatial distribution

1. INTRODUCTION

With the rapid economic development, urbanization and the increase in the number of motor vehicles, air pollution has gradually become one of the major environmental problems in China [1–3]. Among all the types of atmospheric particulate matter, those with aerodynamic equivalent diameter less than or equal to 2.5 μm are called PM2.5. Studies have shown that human exposure to PM2.5, especially for children, can lead to the development of severe respiratory disease at high PM2.5 concentrations [4,5]. An increase in the concentration of fine particles in ambient air may result in a decrease in cardiopulmonary function, myocardial infarction, etc., and may even affect human life expectancy. The

main pollutants of PM2.5 are volatile organic compounds (VOCs), NOx, SO_2, CO and NH_3, which combine with atmospheric particles through photochemical reactions to produce PM2.5 particles. The formation, dispersion and dissipation processes of fine particulate matter pollution are closely related to pollutants and meteorological conditions [6–8]. Therefore, if the distribution state of fine particulate matter and pollutants in the atmosphere before and after the pollution event can be grasped, the correlation between them can be analyzed to provide a reference for the study of the generation process of fine particulate matter, as well as the prediction and control of air pollution [9–16].

UAVs, an emerging technology in recent years, have also been applied in environmental monitoring [17,18]. However, very few monitoring systems have been studied and designed for PM2.5 and its pollutants. Air quality monitoring stations are still the major facilities that are used to obtain PM2.5 and its pollutant concentration data [19]. Many scholars in the atmospheric field intend to study not only the horizontal ground-level concentration distribution, but also the vertical distribution characteristics and interrelationships of pollutants such as PM2.5. However, the analysis of the correlation between PM2.5 and its pollutants with the data from monitoring stations is not satisfactory either [20].

PM2.5 sensors are developed based on the scattering principle of light. The light source can be classified into two types: infrared type and laser type [21,22]. Infrared sensors are slow to start and can only measure particles with a diameter of 1μm or more. In contrast, laser-type sensors are fast-acting and can measure particles as small as 0.3 μm in diameter. Due to the different mechanisms, the accuracy of detecting changes in the concentration of CO, SO_2, NO_2 and O_3 pollutants of PM2.5 in the air is much lower than that of detecting PM2.5 [23–25]. The various gas sensors on the market are basically electrochemical sensors, and the integration of electrochemical sensors into UAVs is a very interesting attempt. This work tested a system for monitoring PM2.5 and its pollutant concentrations [26,27], in which several technical indicators, monitoring functions and operational stability were tested. The data of spatial distribution of PM2.5 and its pollutant concentrations were analyzed and a correlation strength study was made with the statistical Spearman correlation coefficient.

2. SYSTEM AND METHODS

2.1. System structure

A self-developed UAV was adopted as a test platform, the system of which can be divided into two parts, aerial monitoring and ground monitoring. The aerial monitoring includes the UAV mounting platform and the on-board gas monitoring board, which can receive the ground track planning information to achieve the goal of automatic flight and hovering according to the specified route. The airborne gas monitoring board was installed on the UAV carrier platform, and the sensors on board can measure PM2.5, SO_2, NO_2, and CO concentrations, as well as meteorological parameters such as temperature, humidity, and air pressure for reference in the study of the correlation between PM2.5 and pollutants. Figure 1 shows the structure of the system. Mission Planner was used as ground monitoring station software.

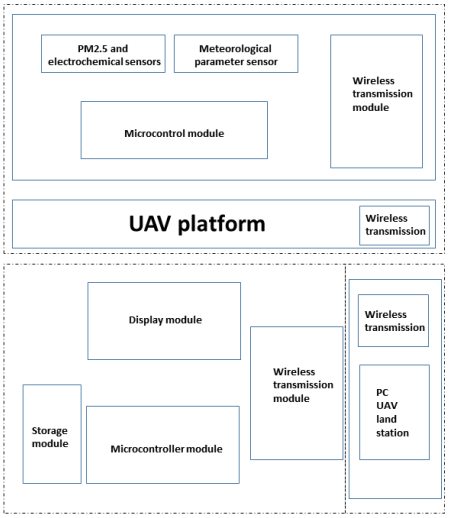

Figure 1. Structure of the UAV system for PM2.5 and pollutants detection.

2.2. Monitoring module structure

Figure 2 illustrates the overall structure of the monitoring module. The microcontroller module on the on-board gas monitoring board communicates with the ground wireless monitoring terminal in both directions through the wireless transmission module. The microcontroller module on the monitoring board is mainly responsible for collecting the data monitored by the sensors and then sending them to the ground microcontroller module through the wireless transmission module. It is peripherally connected to electrochemical CO, SO_2, O_3, NO_2 sensors and PM2.5/PM10 sensors. The portable wireless receiver includes a microcontroller module, a TFT color display, a wireless transmission module and an external SD card module.

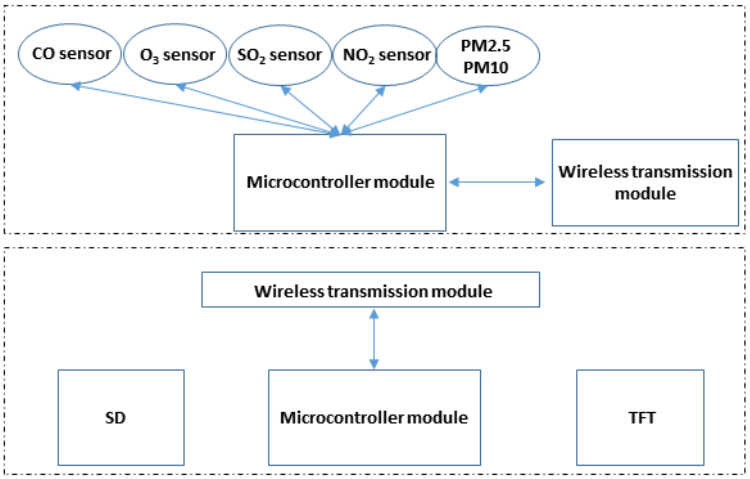

Figure 2. Wireless monitoring module structure of UAV system for PM2.5 and pollutants detection.

2.3. Electrochemical sensors

The electrochemical gas sensors on the market are divided into two categories according to the types of the output signal, which is either analog or digital. The accuracy of sensors with analog output is extremely dependent on the design level of the peripheral circuitry and requires professional calibration. Since the focus of this work is not on small signal amplification, denoising circuit design or sensor calibration, the electrochemical gas sensors with digital output were selected. The electrochemical sensors (CO, SO_2, NO_2, O_3) used in the system were selected from the 7NE series of sensors produced by SerCom Solutions Ltd. Co. The sensors for SO_2, O_3 and NO_2 have a resolution of 1ppb, and the CO sensors have a resolution of 0.01ppm. This paper adopts the approach of sharing a set of microcontroller IO ports to form a serial data bus for multiple serial ports. Each electrochemical sensor has a unique address which is relied on by the sensor to identify each device mounted on the serial bus.

2.4. Airflow shielding test

The electrochemical sensor was installed on the UAV platform and then rested on a flat and clean surface. The power of the on-board sensor, the ground wireless monitoring end and the UAV were all turned on to make sure that they were in working condition. The electrochemical sensor was being warmed up for 1 h and the rotor could not be rotated during this time [28–32]. Afterwards, the store button on the wireless monitor was pressed to start recording all measurements for 1 minute continuously, then the recording was stopped and data set 1 was obtained. The UAV flight control was immediately unlocked and the throttle was pulled to the middle position to keep the rotor at the maximum speed before takeoff. The store button on the wireless monitor was pressed again to start recording all the measurement data for 1 min, then the recording was stopped and data set 2 was obtained.

3. RESULTS AND DISCUSSION

Before the UAV platform took off with electrochemical sensors, the effectiveness of the optimized UAV platform structure needed to be verified. A set of experiments was designed to test the airflow shielding effect of the UAV platform. The two sets of measurements were averaged and the results are shown in Table 1.

Table 1. The average value of each measurement before and after rotation.

Data	PM2.5	PM10	SO_2	NO_2	CO	O_3
Set 1	51.3	64.2	108.4	90.5	0.62	60.5
Set 2	54.8	68.3	109.1	84.6	0.62	60.3

It can be seen from Table 1 that the average value of PM2.5, PM10 and SO_2 increases by 3.5 g/m^3, 4.1 g/m^3 and 0.7 ppb, respectively. The average value of NO_2 and O_3 decreases by 5.9 ppb and 0.2 ppb, respectively. The results show that the data does not show large fluctuations, indicating that the rotor rotation has not exerted much effect on the sensor. Typically, air pollutants can transport down to the ground during the night before, which increases the accumulation of pollutants on the ground, but this process is blocked by the inversion layer and thus the PM2.5 concentrations are higher above the inversion layer than on the ground [33]. The results present that the data does not show any significant fluctuations, indicating that the rotor rotation does not have much influence on the sensor work, with the sensor work bin having the expected effect.

We did 5 groups of tests around Jilin Engineering Normal University and the results are shown in Figure 3-5. It can be seen from the figures that the trend of CO, SO_2 and NO_2 is relatively stable. The peak of CO and SO_2 concentrations on the vertical gradient always occurs at the height near the ground. The concentration of NO_2 increases with the height, while there is a decreasing trend above 500 m. PM2.5 and PM10 decrease and then increase with the increase of height, and then start to decrease again at 400 m. The rising trend from 100-400m may be resulted from the presence of an inversion layer around 400m [34]. In addition, it can be noted that the PM2.5 and PM10 concentration levels at Location 1 are significantly higher than those at Location 2. The real-time meteorological parameters were collected from both locations. It was found that at the same altitude, the humidity in Location 1 was higher and the temperature was lower than that in Location 2. Through comparing pollutant concentrations and meteorological parameters at Location 4 and Location 5, it is found that there was little difference between the values of all monitoring items except humidity. The humidity at Location 4 was always 5-8% lower than that at Location 5 in the vertical direction, which indicates that humidity exerts an important effect on PM2.5. From the pollutant concentrations at each monitoring site, it can be seen that when the average concentration of PM2.5 is high, the average concentrations of CO and SO_2 are at a higher level, and their influence on PM2.5 is more significant. This result is consistent with the result of the research carried out with the unmanned aircraft "ALADINA" [35].

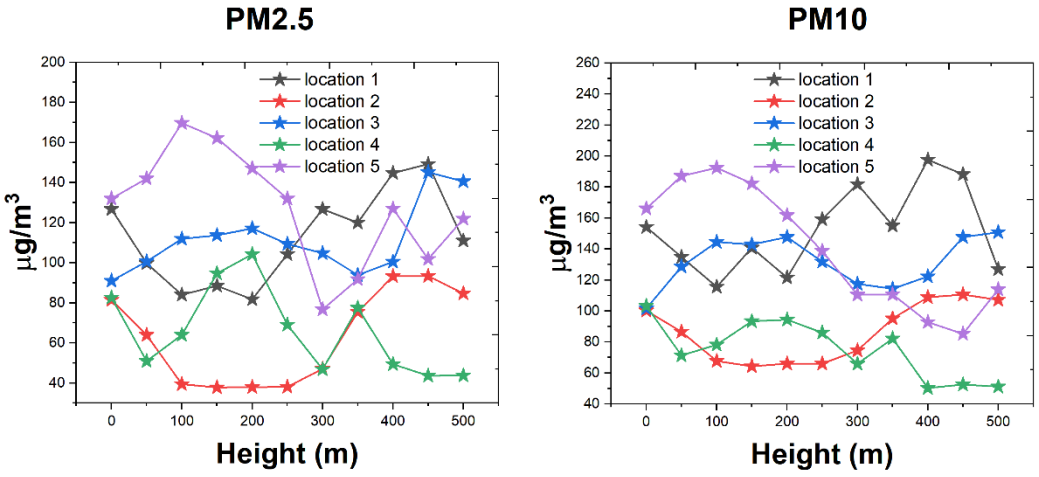

Figure 3. Variation of PM2.5 and PM10 with height.

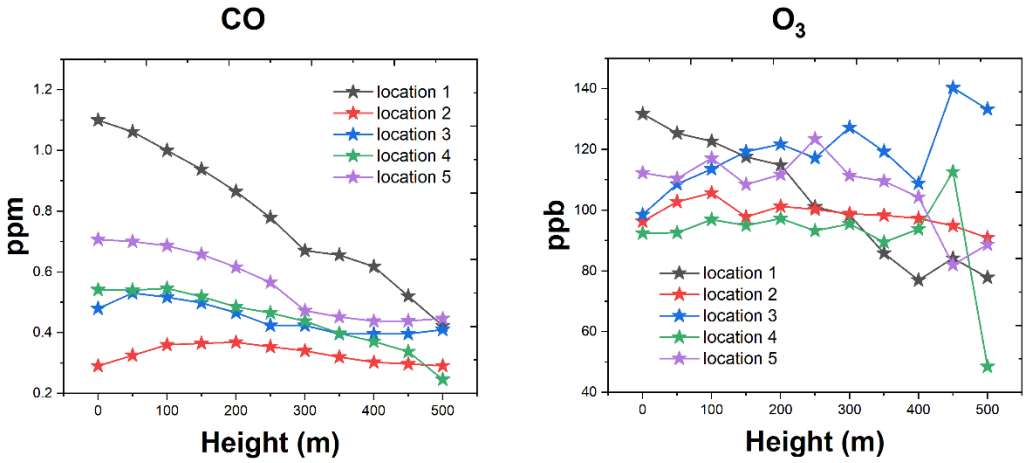

Figure 4. Variation of CO and O_3 concentrations with height.

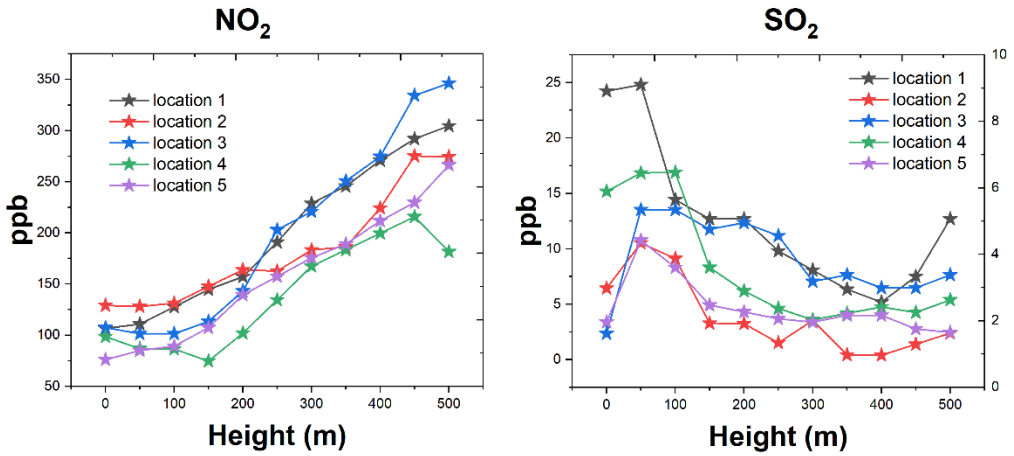

Figure 5. Variation of NO_2 and SO_2 concentrations with height.

Figure 6 shows a scatter plot of the spatial distribution of pollutants for the five groups obtained from this experiment. It is apparent that Locations 4 and 5 have significantly higher overall concentration levels compared to other monitoring sites, the reason for which is that these detection sites are located in industry-intensive areas and commercial centers. The higher SO_2 pollution is mainly concentrated in the boundary layer close to the ground. O_3 is stable and relatively uniform below 350 m, but after the altitude rises above 350m, the concentration starts to be unevenly distributed. On the contrary to SO_2, NO_2 concentration is at a relatively low level in the near-surface region. The thermal inversion is formed due to the heterogeneity of terrain, underlying surface and meteorological conditions, which could produce dynamic and thermodynamic effects towards airflow movements and change the spread condition of air pollutants [36]. The figure presents that the highest NO_2 concentration is in the air around 500m, and the concentration of NO_2 may increase further with the altitude.

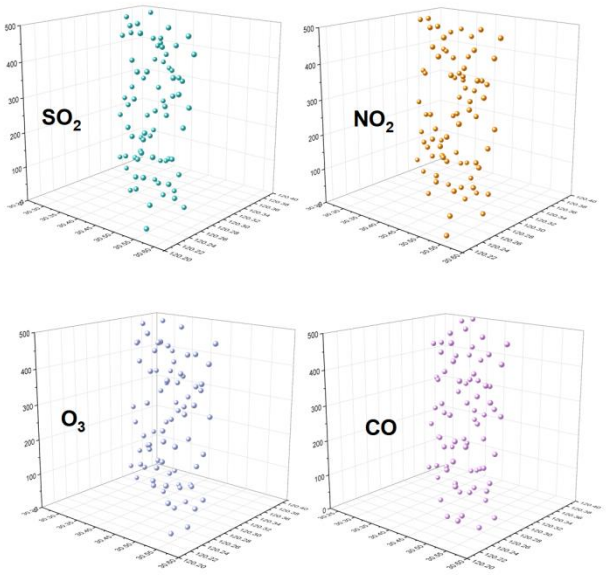

Figure 6. Scatter diagram of spatial distribution of pollutants.

The influence of secondary transformation of gaseous pollutants on the formation and accumulation of PM2.5 has been generally recognized. This work adopts correlation coefficients to analyze this relationship. The strength of the correlation between the independent and dependent variables can be determined by performing Spearman correlation analysis on the data. In this work, SO_2, NO_2, O_3 and CO concentrations were selected as independent variables and PM2.5 concentrations as dependent variables. The vertical distribution of air temperature reflects the stability of the atmospheric structure which impacts the strength of turbulence activity, and governs the spread of air pollution [37]. Wind speed and wind direction were not considered in the correlation analysis because the UAV could not steadily carry wind speed and wind direction instruments. In addition, even if the instruments were mounted on the monitoring platform, it would be difficult to measure the actual wind speed and direction directly due to turbulence resulted from by the motion of the UAV. Therefore, the instrument was used on the ground as an auxiliary measurement to determine the real-time wind speed and direction during the experiment. The calculated results are shown in Table 2.

The Spearman correlation analysis shows that the correlation between CO and PM2.5 concentrations is the strongest, reaching 0.622. O_3 concentrations have the second strongest correlation with PM2.5 concentrations. The weakest relationship is between NO_2 and PM2.5 concentrations with correlation coefficients of -0.187, 0.622 and 0.070, respectively, while, as seen in the table, SO_2 and NO_2 correlation coefficients are positive and they show a positive correlation with PM2.5 concentrations. The correlation was tested for significance at the level of 0.05. Therefore, this study can draw a conclusion that among the pollutants SO_2, NO_2, CO and O_3, CO has the greatest effect on the variation of PM2.5 concentration and the higher the concentration of the pollutant CO is, the higher the concentration of PM2.5 is.

Table 2. Spearman correlation coefficient and P value of PM2.5 and pollutants.

		PM2.5	SO_2	NO_2	CO
SO_2	Correlation coefficient	0.095	-	-	-
	P	0.000	-	-	-
NO_2	Correlation coefficient	0.070	-0.287	-	-
	P	0.002	0.003	-	-
CO	Correlation coefficient	0.622	0.060	-0.127	-
	P	0.002	0.005	0.002	-
O_3	Correlation coefficient	-0.187	0.255	0.061	-0.321
	P	0.000	0.001	0.003	0.002

4. CONCLUSION

In summary, an electrochemical UAV system for PM2.5 and its pollutant concentration monitoring is described in this paper. The spatial distribution of PM2.5 and its pollutants were produced from the data collected at five locations, and the strength of the correlation between PM2.5 and each pollutant was obtained based on the statistical Spearman correlation coefficient.

References

1. W.-Y. Yi, K.-S. Leung, Y. Leung, *Sensors*, 18 (2018) 7.
2. Y. Jiang, P. Liang, X. Huang, Z.J. Ren, *Chemosphere*, 203 (2018) 21–25.
3. L. Zhang, Z. Ren, Z. Su, Y. Liu, T. Yang, M. Cao, Y. Jiang, Y. Tang, H. Chen, W. Zhang, *J. Clin. Endocrinol. Metab.*, 106 (2021) 988–998.
4. G. Kolumban-Antal, V. Lasak, R. Bogdan, B. Groza, *Sensors*, 20 (2020) 403.
5. G. Rohi, G. Ofualagba, *Heliyon*, 6 (2020) e03252.
6. M.A. Zaidan, N.H. Motlagh, P.L. Fung, D. Lu, H. Timonen, J. Kuula, J.V. Niemi, S. Tarkoma, T. Petäjä, M. Kulmala, *IEEE Sens. J.*, 20 (2020) 13638–13652.
7. F. Mao, K. Khamis, S. Krause, J. Clark, D.M. Hannah, *Front. Earth Sci.*, 7 (2019) 221.
8. F. Kizel, Y. Etzion, R. Shafran-Nathan, I. Levy, B. Fishbain, A. Bartonova, D.M. Broday, *Environ. Pollut.*, 233 (2018) 900–909.
9. A.R. Honarvar, A. Sami, *Big Data Res.*, 17 (2019) 56–65.
10. G. Liu, X. Yang, H. Zhang, L. Fu, *Int J Electrochem Sci*, 15 (2020) 5395–5403.
11. J. Ying, Y. Zheng, H. Zhang, L. Fu, *Rev. Mex. Ing. Quím.*, 19 (2020) 585–592.
12. M. Zhang, B. Pan, Y. Wang, X. Du, L. Fu, Y. Zheng, F. Chen, W. Wu, Q. Zhou, S. Ding, *ChemistrySelect*, 5 (2020) 5035–5040.
13. W. Long, Y. Xie, H. Shi, J. Ying, J. Yang, Y. Huang, H. Zhang, L. Fu, *Fuller. Nanotub. Carbon Nanostructures*, 26 (2018) 856–862.
14. Y. Zheng, H. Zhang, L. Fu, *Inorg. Nano-Met. Chem.*, 48 (2018) 449–453.

15. H. Karimi-Maleh, B.G. Kumar, S. Rajendran, J. Qin, S. Vadivel, D. Durgalakshmi, F. Gracia, M. Soto-Moscoso, Y. Orooji, F. Karimi, *J. Mol. Liq.*, 314 (2020) 113588.
16. H. Karimi-Maleh, M. Alizadeh, Y. Orooji, F. Karimi, M. Baghayeri, J. Rouhi, S. Tajik, H. Beitollahi, S. Agarwal, V.K. Gupta, S. Rajendran, S. Rostamnia, L. Fu, F. Saberi-Movahed, S. Malekmohammadi, *Ind. Eng. Chem. Res.*, 60 (2021) 816–823.
17. Q. Yang, Z. Yang, G. Hu, W. Du, *J. Shanghai Jiaotong Univ. Sci.*, 23 (2018) 671–677.
18. H. Kim, W. Kim, S.D. Kim, *Remote Sens.*, 13 (2021) 25.
19. F. Hu, G. Wu, *IEEE Access*, 8 (2020) 93211–93218.
20. J.O. Araujo, J. Valente, L. Kooistra, S. Munniks, R.J. Peters, *Micromachines*, 11 (2020) 768.
21. Y. Tu, M. Bian, Y. Wan, T. Fei, *PeerJ*, 6 (2018) e4858.
22. A. Simic Milas, M. Romanko, P. Reil, T. Abeysinghe, A. Marambe, *Int. J. Remote Sens.*, 39 (2018) 5415–5431.
23. L. Yu, Q. Zhang, D. Jin, Q. Xu, X. Hu, *Talanta*, 197 (2019) 622–630.
24. T. Ito, K. Ogino, K. Nagaoka, K. Takemoto, R. Nishiyama, Y. Shimizu, *JoVE J. Vis. Exp.* (2019) e58371.
25. P. Arroyo, F. Meléndez, S. Rodriguez, J.I. Suárez, S. Carretero, M. Cerrato, E. Pinilla-Gil, J. Lozano, *Sens. Transducers*, 246 (2020) 9–15.
26. C. Jiang, Y. He, Y. Liu, *Analyst*, 145 (2020) 5400–5413.
27. H. Yin, S. Parsnejad, E. Ashoori, H. Wan, W. Li, A.J. Mason, *Microchem. J.*, 168 (2021) 106386.
28. L. Fu, Z. Liu, J. Ge, M. Guo, H. Zhang, F. Chen, W. Su, A. Yu, *J. Electroanal. Chem.*, 841 (2019) 142–147.
29. W. Wu, Q. Zhou, Y. Zheng, L. Fu, J. Zhu, H. Karimi-Maleh, *Int J Electrochem Sci*, 15 (2020) 10093–10103.
30. Q. Liu, Y. Zheng, L. Fu, B.A. Simco, C.A. Goudie, *Aquaculture*, 532 (2021) 735952.
31. J. Zhou, Y. Zheng, J. Zhang, H. Karimi-Maleh, Y. Xu, Q. Zhou, L. Fu, W. Wu, *Anal. Lett.*, 53 (2020) 2517–2528.
32. W. Wu, M. Wu, J. Zhou, Y. Xu, Z. Li, Y. Yao, L. Fu, *Sens. Mater.*, 32 (2020) 2941–2948.
33. Z.-R. Peng, D. Wang, Z. Wang, Y. Gao, S. Lu, *PM25 Res. Yangtze River Delta Obs. Process. Model. Health Eff.*, 123 (2015) 357–369.
34. Z. Zang, W. Wang, W. You, Y. Li, F. Ye, C. Wang, *Sci. Total Environ.*, 575 (2017) 1219–1227.
35. B. Altstädter, A. Platis, B. Wehner, A. Scholtz, N. Wildmann, M. Hermann, R. Käthner, H. Baars, J. Bange, A. Lampert, *Atmos Meas Tech*, 8 (2015) 1627–1639.
36. H.J. Jumaah, B. Kalantar, S. Mansor, A.A. Halin, N. Ueda, S.J. Jumaah, *Drones*, 5 (2021) 60.
37. C. Liu, J. Huang, X.-M. Hu, C. Hu, Y. Wang, X. Fang, L. Luo, H.-W. Xiao, H.-Y. Xiao, *Atmos. Environ.*, 252 (2021) 118332.